Condition for alternans and its control in a two-dimensional mapping model of paced cardiac dynamics

Elena G. Tolkacheva,[1,4] Mónica M. Romeo,[2,4] Marie Guerraty,[2] and Daniel J. Gauthier[1,3,4]
[1]*Department of Physics, Duke University, Durham, North Carolina 27708, USA*
[2]*Department of Mathematics, Duke University, Durham, North Carolina 27708, USA*
[3]*Department of Biomedical Engineering, Duke University, Durham, North Carolina 27708, USA*
[4]*Center for Nonlinear and Complex Systems, Duke University, Durham, North Carolina 27708, USA*
(Received 17 July 2003; published 15 March 2004)

We investigate a two-dimensional mapping model of a paced, isolated cardiac cell that relates the duration of the action potential to the two preceding diastolic intervals as well as the preceding action potential duration. The model displays rate-dependent restitution and hence memory. We derive a criterion for the stability of the 1:1 response pattern displayed by the model. This criterion can be written in terms of experimentally measured quantities—the slopes of restitution curves obtained via different pacing protocols. In addition, we analyze the two-dimensional mapping model in the presence of closed-loop feedback control. The control is initiated by making small adjustments to the pacing interval in order to suppress alternans and stabilize the 1:1 pattern. We find that the domain of control does not depend on the functional form of the map, and, in the general case, is characterized by a combination of the slopes. We show that the gain γ necessary to establish control may vary significantly depending on the value of the slope of the so-called standard restitution curve (herein denoted as S_{12}), but that the product γS_{12} stays approximately in the same range.

DOI: 10.1103/PhysRevE.69.031904 PACS number(s): 87.19.Hh, 87.10.+e, 05.45.−a

I. INTRODUCTION

Several experimental and modeling studies have suggested that an abnormal cardiac rhythm known as alternans of the action potential duration (APD) is a first stage in the development of ventricular arrhythmias [1–5], which often lead to sudden cardiac death. APD alternans is characterized by short-long alternations of the duration of subsequent action potentials and often can be induced by pacing cardiac tissue at a rapid rate.

A well-known mechanism for producing alternans is steep APD restitution, as was first shown theoretically by Nolasco and Dahlen [6]. Guevara *et al.* [7] formularized this concept by modeling the response of cardiac tissue to pacing using the one-dimensional map

$$A_{n+1}=f(D_n). \tag{1}$$

Here, f is the restitution curve (RC), A_{n+1} is the APD generated by the $(n+1)$th stimulus and D_n is the nth diastolic interval (DI), i.e., the interval during which the tissue recovers to its resting state after the end of the previous (nth) action potential. Under pacing at a fixed cycle length, the APD and DI are related through the pacing relation

$$A_n+D_n=B, \tag{2}$$

where B is the pacing interval. It was shown in Ref. [7] that alternans originates via a period-doubling bifurcation and appears whenever the modulus of the slope of the RC is greater than one,

$$|f'|\geqslant 1. \tag{3}$$

The model (1) describing APD as a function of only the preceding DI contradicts many experiments [8–10] which show that the RC depends on the method by which it is measured. Moreover, recent studies [11–15] have shown that the slope of the RC at the onset of alternans can be significantly larger than unity and thus the criterion (3) fails to predict the onset of alternans in some cases.

Based on empirical data, Gilmour and Collaborators [16,17] proposed a different type of mapping model to describe their experiments (later, a model of this form was derived analytically [18] from a three-ionic-current membrane model [19]). They assumed that the APD depends not only on the preceding DI, but also on the preceding APD, so that

$$A_{n+1}=F(A_n,D_n). \tag{4}$$

The mapping model (4) is still a one-dimensional map since the pacing relation (2) holds. However, the explicit dependence of F on both A_n and D_n leads to the fact that the model displays rate-dependent restitution. In particular, the dynamic and $S1$-$S2$ RCs are different (in Sec. III B of this paper we will discuss different types of RCs). The criterion for the existence of alternans for the mapping model (4) was derived by Tolkacheva *et al.* [20]. It predicts that alternans may exist when

$$\left|1-\left(1+\frac{1}{S_{dyn}}\right)S_{12}\right|\geqslant 1. \tag{5}$$

This criterion depends not only on the slope of the dynamic RC S_{dyn} but also on the slopes of the entire family of $S1$-$S2$ RCs S_{12} obtained at different $S1$ pacing intervals.

A focus of recent theoretical and experimental studies is to understand the mechanisms causing alternans and to terminate this response pattern using closed-loop feedback methods developed by the nonlinear dynamics community. Over the past few years, several studies have demonstrated

that alternans can be suppressed with dynamic feedback control of the pacing interval [21–25]. Recently, Hall *et al.* [24] demonstrated successful control of alternans in small pieces of *in vitro* paced bullfrog ventricles. Their experiments demonstrated that alternans could be suppressed over a wide range of control parameters and over the entire range of pacing rates for which alternans was observed. However, poor agreement between the experimental data and the theoretical models was observed, fitting the bifurcation diagrams of the mathematical models to the experimental data did not produce good fits for the observed domains of control. Specifically, control of alternans was observed for feedback gains as large as four in the experiments, whereas the models predicted that the gain must be less than ~ 0.4 and limited to a small region of pacing rates near the bifurcation to alternans.

The control of alternans in the mapping models (1) and (4) was considered in Ref. [26]. Basically, it was shown that (1) the domain of control does not depend on the specific functional form of f and F but only on the value of its derivatives at the fixed point and (2) the domain of control for the mapping model (4) is regulated by S_{12}. Indeed, the analysis made in Ref. [26] indicates that the mapping model (1) does not agree with the experiment and the mapping model (4) may, in principle, describe the experimentally observed domain of control if S_{12} is truly less than one (as, for instance, in bullfrogs).

Several experimental and theoretical studies [14–17,27–29] indicate that the memory effects have to be taken into account in order to explain the more complex dynamics found in small cardiac cells. These effects were modeled by introducing a new variable M_n in a two-dimensional mapping model of the form

$$A_{n+1}=p(D_n,M_{n+1}), \tag{6a}$$

$$M_{n+1}=g(A_n,D_n,M_n). \tag{6b}$$

The model (6) can be equivalently expressed as

$$A_{n+1}=\Phi(A_n,D_n,D_{n-1}). \tag{7}$$

Expressing the mapping model (6) in the form of Eq. (7) shows that introducing the variable M_n obscures the fact that the ''memory'' in these models just consists of an explicit dependence on the second-to-the-last DI, in addition to its dependence on the last DI and APD. This is in contrast to Eq. (1), where APD only depends on the preceding DI, and Eq. (4), where the APD depends on the preceding APD and DI. The dependence of the APD not only on the preceding DI but also on the previous APD and earlier DI indicates, in general, the presence of short memory in the model. Accordingly, the mapping model (4) has one beat of memory and the mapping model (7) has two beats of memory. Including one more beat of memory can change dramatically the dynamic properties of the model [30]. In particular, the mapping model (7) can exhibit (under a certain parameter range) the so-called APD accommodation effect [27,30], where it takes up to several minutes for the APD to reach a steady-state value under periodic pacing. The presence of memory along with electrotonic effects can affect the appearance of alternans in the isolated cardiac cell [13,15,31].

Note that the memory effects described by mapping models (4) and (7) are associated with a history of pacing over some period of time, as have been defined in the Ref. [28]. Within this definition, the mapping models (4) and (7) refer to memory effects of the order of several seconds and up to several minutes, respectively.

In this paper we investigate the stability and control of alternans in the two-dimensional mapping model (7). In Sec. II, we derive the expression (7) and present a typical bifurcation diagram for a particular form of the function Φ. In Sec. III, we derive a generic bifurcation criterion for the existence of alternans in the two-dimensional mapping model (7). We show that it can be written in terms of quantities that can be measured experimentally (slopes of different types of RCs). In Sec. IV, we investigate control of alternans in the two-dimensional mapping model (7) and determine the region where control is successful.

II. TWO-DIMENSIONAL MAPPING MODEL

To derive the expression (7), we use Eq. (6a) for the nth stimulus

$$A_n=p(D_{n-1},M_n) \tag{8}$$

to solve for M_n,

$$M_n=\tilde{p}(D_{n-1},A_n). \tag{9}$$

Then we substitute Eq. (9) into Eq. (6b) and that, in turn, is substituted into Eq. (6a) to obtain

$$A_{n+1}=p[D_n,g(A_n,D_n,\tilde{p}(D_{n-1},A_n))]\equiv\Phi(A_n,D_n,D_{n-1}). \tag{10}$$

Since the variables A_n and D_n are dependent through the pacing relation (2), Eq. (10) is simply a second-order difference equation in the variable A_n. By introducing a new variable, Eq. (10) can be rewritten as a two-dimensional system of first-order difference equations.

The general form of the mapping model (6) includes the model described by Chialvo, Michaels, and Jalife [28] as well as the model described by Fox, Bodenschatz, and Gilmour [14]. Both models are of the particular form

$$A_{n+1}=(1-\alpha M_{n+1})G(D_n), \tag{11a}$$

$$M_{n+1}=[1-(1-M_n)e^{-A_n/\tau_2}]e^{-D_n/\tau_2}, \tag{11b}$$

where

$$G(D_n)=A+\frac{E}{1+e^{-(D_n-C)/D}} \tag{12}$$

in the Fox *et al.* model [14], and

$$G(D_n)=a_1-a_2e^{-D_n/\tau_1} \tag{13}$$

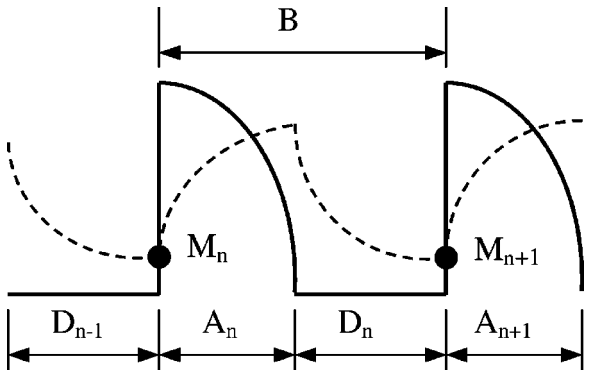

FIG. 1. Schematic representation of memory accumulation (during the action potential duration) and dissipation (during the diastolic interval) in the two-dimensional mapping model (7).

in the Chialvo *et al.* model [28] ($\alpha=1$). Here $A,C,D,E,a_1,a_2,\tau_1,\tau_2$ are tissue-dependent parameters. Note that the mapping model (11) can be easily rewritten in the form (7).

Figure 1 is a schematic representation of the APD, DI, and the memory variable M shown for the mapping model (11). The memory variable M accumulates during the duration of the action potential and dissipates during the diastolic interval. Figure 1 shows all the relevant variables for both ways of expressing the two-dimensional mapping model: by Eqs. (6) or by Eq. (7), and the relationships among them.

For the remainder of this article, we discuss the system of interest (6) in the more manageable form of Eq. (7). However, since Eqs. (6) are equivalent to Eq. (7), all the results presented herein are applicable to Eqs. (6). To illustrate our results, we use the Fox *et al.* mapping model given by Eqs. (11), (12) with a specific set of parameters that were chosen in Ref. [14] to produce good qualitative agreement with data generated by an ionic model simulation. This ionic model was developed earlier [32] to describe experimental data representing dynamics of the canine ventricular myocytes. A typical bifurcation diagram for this particular mapping model is presented in Fig. 2. In order to obtain the diagram, the Eqs. (11), (12) were iterated at each pacing interval B until the APD reached the steady-state value A^*. Note that the tissue has a stable 1:1 response pattern (every stimulus elicits an action potential of equal duration) for long pacing intervals (slow pacing rate). As the pacing interval decreases (faster pacing), the 1:1 response becomes unstable and a transition to alternans (2:2 response) occurs. At faster pacing rates, the 1:1 response pattern becomes stable again. For the 1:1 and 2:2 responses considered herein, the pacing relation (2) holds.

III. STABILITY OF THE TWO-DIMENSIONAL MAPPING MODEL

In this section we analyze stability of the 1:1 response pattern in the two-dimensional mapping model (7) [equivalently, Eqs. (6)] and derive a criterion for the existence of alternans (2:2 response pattern). We introduce the different types of RCs and express the criterion in terms of experimentally measured quantities—the slopes of these RCs.

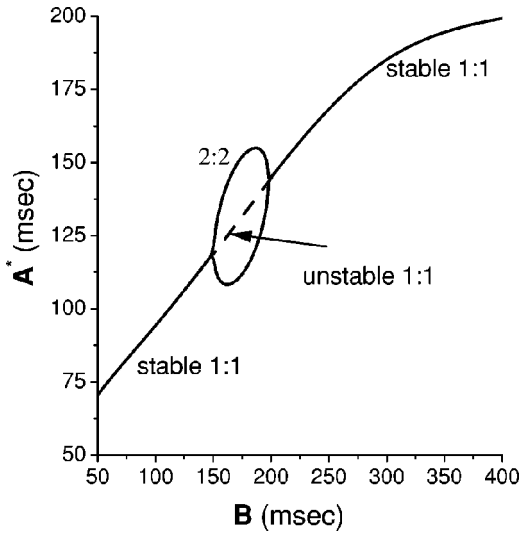

FIG. 2. Bifurcation diagram showing existence of alternans (2:2 response pattern) in the Fox *et al.* model [14]. The model parameters are: $A=88$ msec, $E=122$ msec, $C=40$ msec, $D=28$ msec, $\tau_2=180$ msec, and $\alpha=0.2$. Alternans occur within the range of pacing intervals from 150 msec to 200 msec. Note that in this range the 1:1 response pattern is unstable, as is indicated by the dashed line. The solid curves denote stable behavior.

A. Stability region

To find a stability region for the two-dimensional mapping model, we linearize Eq. (7) in a neighborhood of the fixed point A^*,

$$A_{n+1}=A^*+D_1\Phi|_{f.p.}(A_n-A^*)+D_2\Phi|_{f.p.}(D_n-D^*)+D_3\Phi|_{f.p.}(D_{n-1}-D^*), \tag{14}$$

where $D_i\Phi$ is the derivative of Φ with respect to its ith argument, *f.p.* denotes evaluation at the fixed point A^*, and $D^*=B-A^*$.

Using new parameters representing deviations from the fixed point

$$\delta_n=A_n-A^*, \quad \alpha_n=\delta_{n-1}, \tag{15}$$

we can rewrite expression (14) in the form

$$\begin{pmatrix}\delta_{n+1}\\ \alpha_{n+1}\end{pmatrix}=\begin{pmatrix}\mu & -\rho\\ 1 & 0\end{pmatrix}\begin{pmatrix}\delta_n\\ \alpha_n\end{pmatrix}, \tag{16}$$

where

$$\mu\equiv D_1\Phi|_{f.p.}-D_2\Phi|_{f.p.}, \quad \rho\equiv D_3\Phi|_{f.p.}. \tag{17}$$

The eigenvalues of the 2×2 matrix given in Eq. (16) are

$$\lambda_{1,2}=\frac{1}{2}(\mu\pm\sqrt{\mu^2-4\rho}), \tag{18}$$

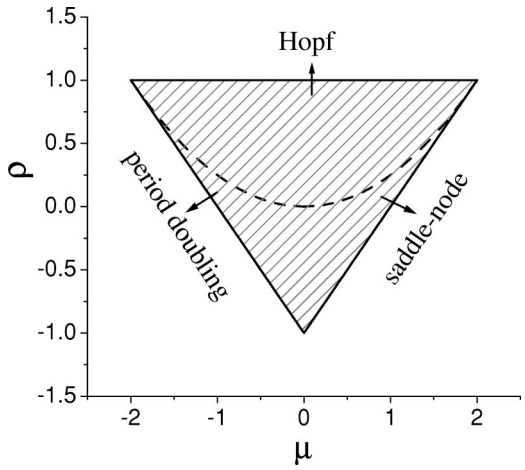

FIG. 3. Stability region (the region inside the triangle) for the two-dimensional mapping model (7) given by Eq. (19). The dashed curve represents the boundary between the regions where the eigenvalues are real (below the dashed line) and complex (above the dashed line). Arrows indicate the three possible types of bifurcations that occur when the system loses stability.

so the fixed point A^* is stable when $|\lambda_{1,2}|<1$. This occurs when μ and ρ lie within the triangular region defined by the lines

$$\rho=1, \quad \rho-\mu=-1, \quad \text{and} \quad \rho+\mu=-1. \tag{19}$$

Figure 3 displays the region of stability given in Eq. (19). The dashed curve corresponds to the expression $\mu^2-4\rho=0$ that represents the boundary between real and complex eigenvalues: the eigenvalues above (below) the dashed curve are complex conjugates (real). As seen in Fig. 3, different types of bifurcations may occur when the system loses stability. Typically, when an eigenvalue λ crosses $\{\lambda=1\}$, a saddle-node bifurcation occurs [33]. When a complex-conjugate pair of eigenvalues crosses the unit circle, then generally a Hopf bifurcation occurs [33]. In this paper, we are interested in a period-doubling bifurcation because it corresponds to the appearance of alternans [7,14]. Since this bifurcation usually occurs when one of the eigenvalues passes through -1,

$$C(\mu,\rho)\equiv\mu+\rho=-1 \tag{20}$$

is the condition where stable 1:1 behavior may bifurcate to alternans in the two-dimensional mapping model (7).

B. Bifurcation criterion: Connection with slopes of different types of RCs

The condition for existence of alternans Eq. (20) contains two quantities μ and ρ, which, because of the greater complexity of the model, are difficult to connect with quantities having significant physical meaning. In this section, we express criterion (20) in terms of quantities that can be measured experimentally. Experimentally, a RC can be obtained by plotting APD as a function of the preceding DI according to a particular pacing protocol. Using different pacing protocols it is possible to obtain different RCs and measure their slopes. Below, we determine the slopes of the $S1$-$S2$, dynamic and constant-BCL RCs (following Ref. [20] where the main types of RCs were defined) based on the two-dimensional mapping model (7) and express criterion (20) in terms of these slopes.

1. S1-S2 RC

The $S1$-$S2$ RC (also known as the standard RC) is obtained by pacing the preparation at a given pacing interval $S1$ until the steady state (A^*,D^*) is reached, and then adding a single premature stimulus after a particular DI $D_{S_1S_2}$ (at pacing interval $S2$). The full $S1$-$S2$ RC is determined by measuring the resulting APD $A_{S_1S_2}$ for various DIs $D_{S_1S_2}$. Note that for each S1 there is only one $S1$-$S2$ RC. According to this protocol, the mapping model (7) can be rewritten using $A_{n+1}=A_{S_1S_2}$ in the following form:

$$A_{S_1S_2}=\Phi(A^*,D_{S_1S_2},D^*) \tag{21}$$

because all APDs and DIs except the last ones are the same, since steady state has been reached. The slope of the $S1$-$S2$ RC evaluated at the fixed point A^* can be found from the expression (21) as

$$S_{12}=\left.\frac{dA_{S_1S_2}}{dD_{S_1S_2}}\right|_{S1=S2}=D_2\Phi|_{f.p.}. \tag{22}$$

2. Dynamic RC

The dynamic (steady state) RC is obtained by pacing the preparation at a fixed pacing interval until steady state is reached, at which time a single pair (A^*,D^*) is recorded. The process is repeated for decreasing pacing intervals. During alternans, the last two (A^*,D^*) pairs are recorded so that both the short and long action potentials are included. In order to determine stability of the 1:1 response, let us consider the dynamic RC without alternans. In this case at steady state, expression (7) can be rewritten in the following form:

$$A^*=\Phi(A^*,D^*,D^*), \tag{23}$$

which can be used to determine the slope of the dynamic RC,

$$S_{dyn}\equiv\frac{dA^*}{dD^*}=D_1\Phi|_{f.p.}\frac{dA^*}{dD^*}+D_2\Phi|_{f.p.}+D_3\Phi|_{f.p.}. \tag{24}$$

Combining Eqs. (17), (22), and (24), we can determine μ as

$$\mu=1-S_{12}-\frac{S_{12}+\rho}{S_{dyn}}. \tag{25}$$

3. Constant-BCL RC

The constant-BCL RC [17,20] describes the transient response of the paced cardiac tissue for a constant BCL, as it approaches the steady-state value following a change in

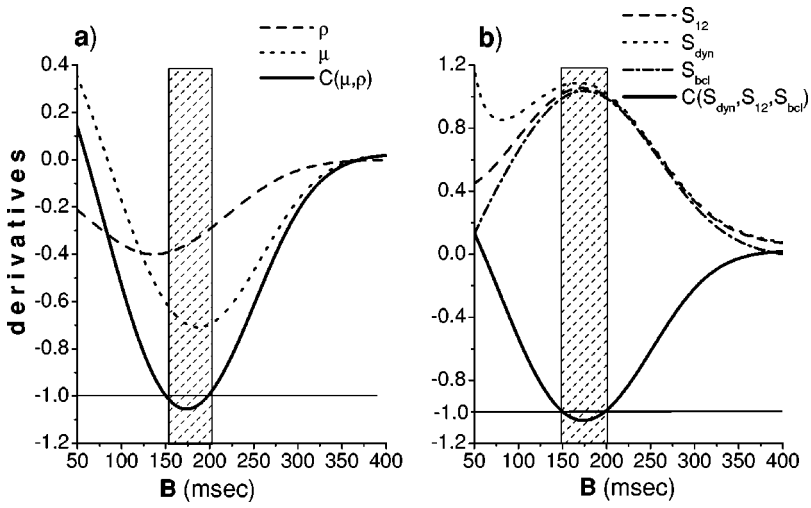

FIG. 4. Illustrations of the bifurcation criterion corresponding to the bifurcation diagram in Fig. 2 in terms of (a) values of μ and ρ and (b) slopes of different RCs S_{dyn}, S_{12}, S_{bcl}. The solid horizontal line is equal to -1. The region between the solid vertical lines is the region where alternans exist according to the bifurcation diagram (Fig. 2). Note that $C=-1$ at the onset of alternans.

BCL. A pacing protocol that allows the measurement of the slopes S_{12}, S_{dyn}, and S_{bcl} [34] of all RCs at each fixed point is described in Ref. [20].

As was shown in Ref. [20], the slope of the constant-BCL RC S_{bcl} is equal to the full derivative (with negative sign) of the expression (7) calculated at the fixed point:

$$S_{bcl} \equiv -\frac{d\Phi}{dA_n} = -\left(D_1\Phi + D_2\Phi \frac{dD_n}{dA_n} + D_3\Phi \frac{dD_{n-1}}{dA_n} \right)\Bigg|_{f.p}. \tag{26}$$

Realizing that $dD_n/dA_n = -1$, and $dA_n/dD_{n-1} \simeq S_{12}$, and taking into account Eq. (17), we can rewrite Eq. (26) as

$$S_{bcl} = -\mu - \frac{\rho}{S_{12}}. \tag{27}$$

Finally, the following expression for ρ is derived from Eqs. (25) and (27):

$$\rho = \frac{S_{12}S_{dyn}}{S_{dyn}-S_{12}} \left(\frac{S_{12}}{S_{dyn}} - 1 + S_{12} - S_{bcl} \right), \tag{28}$$

and thus the *bifurcation criterion* (20) containing the slopes of the different types of RC is

$$C(S_{dyn},S_{12},S_{bcl}) \equiv \left(1 - S_{12} - \frac{S_{12}}{S_{dyn}} \right) + \frac{S_{12}(1-S_{dyn})}{S_{dyn}-S_{12}} \times \left[\left(1 - S_{12} - \frac{S_{12}}{S_{dyn}} \right) + S_{bcl} \right] = -1. \tag{29}$$

Criterion (20) determines the bifurcation of the 1:1 response pattern of the two-variable mapping model (7) in terms of μ and ρ. Criterion (29) contains the same information in terms of the experimentally measured quantities S_{dyn}, S_{12}, and S_{bcl}. Equations (25) and (28) give the relationship between all these variables. For emphasis, we are using the same symbol C to refer to both the function $C(\mu,\rho)$, when the bifurcation criterion (20) is expressed in terms of derivatives of Φ, *and* to the function $C(S_{dyn},S_{12},S_{bcl})$, when that same criterion is expressed in terms of slopes of the RCs as in Eq. (29).

In Fig. 4, the stability criterion expressed by Eqs. (20) and (29) together with the values of μ,ρ,S_{dyn}, S_{12}, and S_{bcl} are presented for different values of the pacing intervals corresponding to the bifurcation diagram in Fig. 2. Comparing Figs. 2 and 4 show that the transition to alternans does indeed occur as predicted by Eqs. (20) and (29). For this particular set of parameters, S_{dyn}, S_{12}, and S_{bcl} are close (but not equal) to unity at both the onset and the offset of alternans. However, μ and ρ are far from unity at these points.

IV. CONTROL OF ALTERNANS IN THE TWO-DIMENSIONAL MAPPING MODEL

The key idea underlying the control of alternans is to design perturbations that stabilize the system about an unstable equilibrium state. In our analysis, the unstable equilibrium state is the 1:1 pattern for which the APD is the same for each stimulus and equal to A^*. The experimental results of Ref. [21] show that measuring the APD, then making small, real-time adjustments to the pacing interval—once per cycle—can stabilize the unstable equilibrium state in small pieces of in vitro paced bullfrog cardiac muscle. In those experiments, for each pacing interval, the response of the tissue to the first 5–10 stimuli was discarded in order to eliminate transients and only the steady-state values of the APD were recorded. The duration of each action potential was determined at 70% of full repolarization. Following Ref. [21], we adjust the pacing interval B by the small amount

$$\varepsilon_n = -\gamma(A_{n-1} - A_{n-2}), \tag{30}$$

where γ is the feedback gain. Applying this control to the mapping model (7) yields the controlled system

$$A_{n+1} = \Phi(A_n, D_n, D_{n-1}, \varepsilon_n, \varepsilon_{n-1}),$$

$$\varepsilon_{n+1} = -\gamma(A_n - A_{n-1}). \tag{31}$$

By linearizing Eq. (31) about the fixed point (when $A_n = A^*$ and $\varepsilon_n = 0$), using Eq. (15) and introducing the new parameters

$$e_n = \varepsilon_n / \gamma, \quad \theta_n = \varepsilon_{n-1} / \gamma, \tag{32}$$

we obtain

$$\begin{pmatrix} \delta_{n+1} \\ e_{n+1} \\ \theta_{n+1} \\ \alpha_{n+1} \end{pmatrix} = \begin{pmatrix} \mu & \gamma S_{12} & \gamma\rho & -\rho \\ -1 & 0 & 0 & 1 \\ 0 & 1 & 0 & 0 \\ 1 & 0 & 0 & 0 \end{pmatrix} \begin{pmatrix} \delta_n \\ e_n \\ \theta_n \\ \alpha_n \end{pmatrix} \tag{33}$$

because by definition

$$\left.\frac{\partial \Phi}{\partial \varepsilon_{n-1}}\right|_{f.p.} = \rho, \quad \left.\frac{\partial \Phi}{\partial \varepsilon_n}\right|_{f.p.} = S_{12}. \tag{34}$$

Equation (33) indicates that the domain of control for the two-dimensional mapping model (7) does not depend on the specific functional form of Φ, but only on the value of its derivatives evaluated at the fixed point and the feedback gain γ. Since the stability of the fixed point depends nontrivially on four parameters (μ, ρ, S_{12}, γ), the domain of control is four dimensional and cannot be easily visualized. In comparison, the domains of control for the one-dimensional mapping models (1) and (4) also do not depend on the specific functional form of f and F, but they are characterized by only two parameters (μ,γ) and ($\mu, \gamma S_{12}$), respectively. See Ref. [26] to view these two-dimensional graphs.

To determine the possible boundaries of the volume in (μ,ρ,S_{12},γ) space where the fixed point of the controlled system is stable we use the characteristic equation of the system in Eq. (33),

$$\lambda^4 - \lambda^3\mu + \lambda^2(\rho + \gamma S_{12}) + \lambda\gamma(\rho - S_{12}) - \gamma\rho = 0, \tag{35}$$

where λ denotes an eigenvalue of Eq. (33). Possible boundaries of the domain of control are the surfaces where the modulus of at least one of the eigenvalues equals one. In other words, the stability of a fixed point may only change if an eigenvalue λ crosses the unit circle. If the eigenvalue is real then it could pass through $\lambda = 1$ or $\lambda = -1$; if the eigenvalue is complex, then it and its complex conjugate could move through $\lambda = e^{\pm i\theta}$ for some $\theta \in [0, 2\pi]$. Each of these conditions yields a codimension-one surface. Let Σ_1 be all the (μ,ρ,S_{12},γ) values that yield an eigenvalue $\lambda = 1$; Σ_2 corresponds to those parameter values where $\lambda = -1$; and Σ_3 is the set of all values where $\lambda = e^{\pm i\theta}$. We find each of these surfaces by substituting the corresponding value of λ into Eq. (35). For $\lambda = \pm 1$, this is a straightforward calculation. For $\lambda = e^{\pm i\theta}$, we find the surface Σ_3 by first noting that the left-hand side of Eq. (35) factors into

$$\begin{aligned}(z - e^{i\theta})(z - e^{-i\theta})(z^2 + c_2 z + c_3) \\ = (z^2 + c_1 z + 1)(z^2 + c_2 z + c_3),\end{aligned} \tag{36}$$

where $c_i \in R$ for $i = 1,2,3$. Expanding this product yields

$$z^4 + (c_1 + c_2)z^3 + (1 + c_1 c_2 + c_3)z^2 + (c_2 + c_1 c_3)z + c_3. \tag{37}$$

We equate the coefficients of Eqs. (35) and (37) to find the condition for Eq. (35) to have at least two complex conjugate roots of modulus one.

The surfaces are

$$\Sigma_1 = \{(\mu,\rho,S_{12},\gamma) \,|\, \mu - 1 - \rho = 0\}, \tag{38}$$

$$\Sigma_2 = \{(\mu,\rho,S_{12},\gamma) \,|\, \mu + 1 + \rho - 2\gamma(\rho - S_{12}) = 0\}, \tag{39}$$

$$\Sigma_3 = \{(\mu,\rho,S_{12},\gamma) \,|\, \rho + \gamma S_{12} + \gamma\rho - \mu V - 1 + V^2 = 0\}, \tag{40}$$

where

$$V = \frac{\gamma(\rho - S_{12}) + \mu}{1 + \gamma\rho}. \tag{41}$$

Only a subset of the surfaces Σ_1, Σ_2, and Σ_3 serve as boundaries for the domain of control. The reason is that the stability of the fixed point need not change as an eigenvalue crosses Σ_i. For example, an eigenvalue crossing the unit circle does not change the stability of the fixed point if there is already another eigenvalue with modulus greater than one. In this case, the fixed point will remain unstable.

To determine the regions bounded by Σ_i, $i = 1,2,3$, where all the eigenvalues have modulus less than one, we numerically compute the maximum eigenvalue of Eq. (33) at each point in the space. This allows us to differentiate between regions where the fixed point of the controlled system is stable, and those where it is unstable (i.e., there exists an eigenvalue with modulus greater than one).

As seen in Eq. (19) the stability of the uncontrolled system depends only on μ and ρ. When we add control, the additional parameters S_{12} and γ are introduced. Thus, the domain of control is four-dimensional. To present the domain we first fix the parameter S_{12} (at the values 0.2, 1, and 1.5) because it is the only tissue-dependent parameter that does not explicitly play a role in the stability of the uncontrolled system. In choosing the particular values of S_{12}, we took into account the following: for typical parameter values, as listed in Fig. 2, $S_{12} \simeq 1$ at the onset of alternans (see Fig. 4). Furthermore, some experiments show that S_{12} could be very small [30,35] or greater than one [8] in actual tissue.

Fixing S_{12}, we compute the eigenvalues and calculate the possible boundaries $\Sigma_i, i = 1,2,3$, for μ values in the range $[-3,3]$, with a step size of 0.05. For each value of μ, we find the region where all the eigenvalues have modulus less than one and record the maximum range of ρ and γ corresponding to that region. The range of ρ for which control is possible [i.e., there exists some γ for which all the eigenvalues of Eq. (35) are less than one] is displayed in subplots (a), (c), and (e) of Fig. 5 as regions enclosed by the solid lines. Similarly, the range of γ for which control is successful is presented in subplots (b), (d), and (f) of Fig. 5. For a given set of parameters (μ,ρ,S_{12}), the left column in Fig. 5 shows the range where control is possible. The corresponding subplot on the right gives a possible range of γ which can be applied in

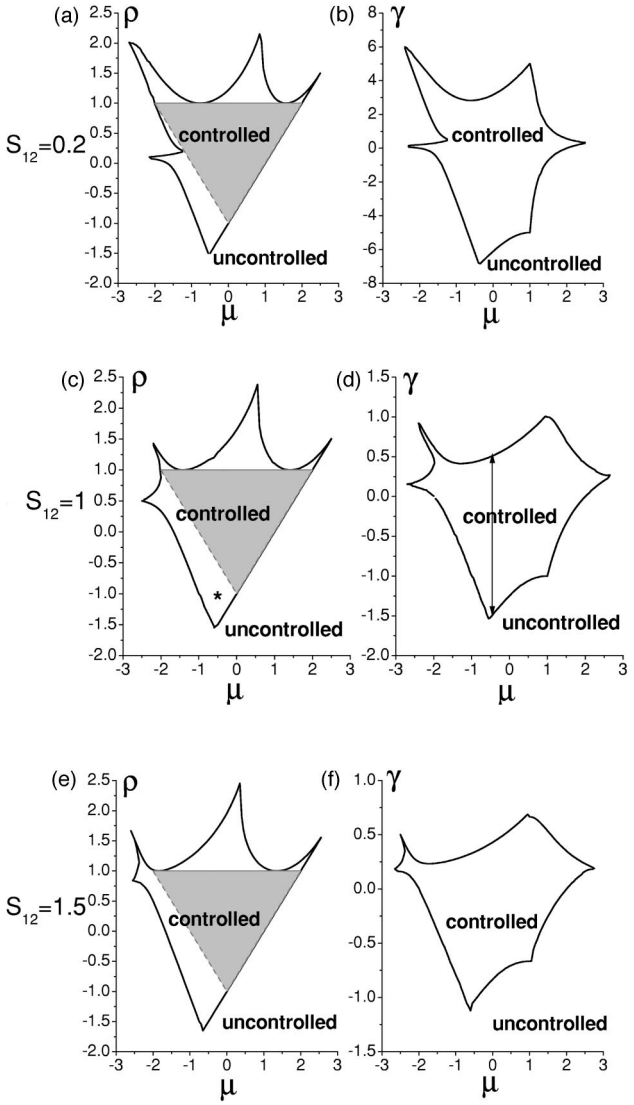

FIG. 5. Domains of control (regions enclosed by the solid lines) for $S_{12}=0.2$, 1, and 1.5. Subplots (a), (c), and (e) show the values of (μ,ρ) where control is possible, i.e., there exists some value of γ which stabilizes the fixed point. Outside of these regions, the fixed point cannot be stabilized for any value of γ. The shaded triangular region of stability for the uncontrolled map is included for comparison. Subplots (b), (d), and (f) show for which values of γ the fixed point can be stabilized.

order to establish the control. For example, for $\mu=-0.5$, $\rho=-1$, and $S_{12}=1$ [this point is shown as an asterisk in Fig. 5(c)], control can be achieved for some values of $\gamma\in(-1.5,0.5)$ [denoted by an arrow in Fig. 5(d)].

Figure 5 shows that the domains of control are qualitatively similar for different values of S_{12}. However, the minimum and the maximum values of γ differ significantly: for instance, $\gamma\in(-1.2,0.7)$ for $S_{12}=1.5$, whereas $\gamma\in(-7,6)$ for $S_{12}=0.2$. The range of γ is larger (smaller) for the smaller (larger) values of S_{12}. This suggests that perhaps it is the product γS_{12}, rather than the individual values of γ and S_{12}, that is the relevant quantity. Note that the domain of control for the mapping model (4) depends on this same quantity

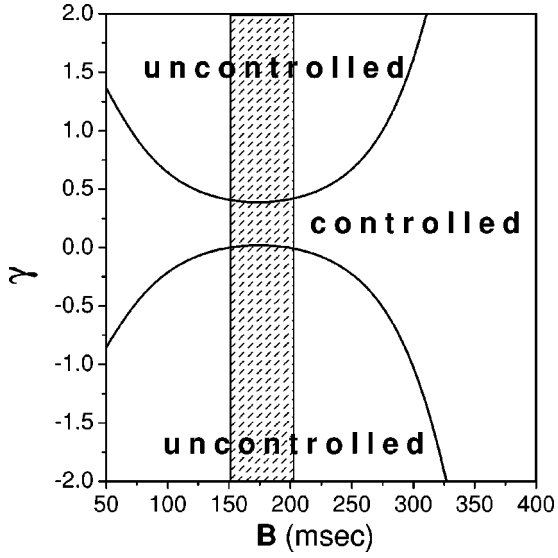

FIG. 6. Domain of control of alternans for the Fox *et al.* model [14] for specific values of parameters from Fig. 2. The shaded region between the two vertical lines indicates the range where alternans exists in the absence of control.

γS_{12} [26]. Recall that S_{12} is the slope of the $S1$-$S2$ RC evaluated at each point of the dynamic RC, i.e., for different values of S1. From the physical point of view, S_{12} quantifies the response of the tissue (in equilibrium) to a sudden perturbation, which the controller attempts to cancel.

For the purpose of illustration, we calculated the domain of control using the once-per-cycle control scheme for the particular case of the Fox *et al.* mapping model [14] given by Eqs. (11), (12) with the parameters listed in Fig. 2. First, we determine the values of μ, S_{12} and ρ for each value of the pacing interval B, as shown in Fig. 4. Then, using Eqs. (39) and (40), for each B we can find the value of the feedback gain γ for which control is possible. Our results are presented in Fig. 6 where the controlled and uncontrolled regions are shown. The shaded region between the two vertical lines indicates the range where alternans exists in the absence of control. Figure 6 demonstrates that the value of the gain γ necessary to establish control is relatively small ($0<\gamma<0.4$) at the onset and the offset of alternans.

Comparing our predictions to experiments is not possible at this time because no experiments have measured the slopes of the different RCs evaluated at the fixed point. A pacing protocol for determining the slopes of different RCs at the fixed point is proposed in Ref. [20] and implemented experimentally in Ref. [30]. Results presented in Ref. [30] for bullfrog cardiac muscle indicate, in particular, that S_{12} can be very small (as small as 0.05) and, thus, according to Fig. 5(b), the gain necessary to establish control could be quite large.

V. CONCLUSION

To predict the onset of alternans in an isolated cardiac cell, a two-dimensional map of the form (6) is expressed as Eq. (7) and the relevant derivatives are calculated.

The bifurcation to alternans occurs according to the criterion (20). Alternatively, this criterion is expressed in Eq. (29) in terms of experimentally measured quantities—the slopes of different restitution curves S_{dyn}, S_{12}, and S_{bcl}. Furthermore, the two-dimensional mapping model (7) is analyzed in the presence of closed-loop feedback control in order to suppress alternans. We find that the parameter region where alternans can be suppressed and the cardiac cell's 1:1 response pattern can be stabilized is a four-dimensional volume in the parameter space $(\mu, \rho, S_{12}, \gamma)$. We show that the domain of control does not depend on the specific functional form of the map and, in the general case, is characterized by a combination of the slopes of different types of RCs. We present projections of the domain of control for different values of S_{12} (that could be observed experimentally). We calculate the gain γ for which control is successful and conjecture that the relevant quantity for stabilizing the 1:1 response pattern in cardiac tissue is the product γS_{12} rather than the individual values of γ and S_{12}.

The analysis we present can be generalized to maps of the form $A_{n+1}=\Phi(A_n, D_n, A_{n-1}, D_{n-1}, \ldots, A_{n-m}, D_{n-m})$, where $m<n$. This might correspond to a cardiac cell that has higher-dimension memory. The difficulty, however, is that the domain of control of the resulting higher-dimensional system will be tractable only with the help of numerical methods.

ACKNOWLEDGMENTS

We gratefully acknowledge the support of the National Science Foundation under Grants Nos. PHY-9982860, PHY-0243584, National Institutes of Health under Grant No. 1R01-HL-72831 (E.G.T. and D.J.G.), and the National Science Foundation under Grant No. DMS-9983320 (M.M.R. and M.G.), as well as fruitful discussion with Professor David Schaeffer.

[1] A. Karma, Chaos **4**, 461 (1994).
[2] M.A. Watanabe, N.F. Otani, and R.F. Gilmour, Jr., Circ. Res. **76**, 915 (1995).
[3] R.F. Gilmour, Jr. and D.R. Chialvo, J. Cardiovasc. Electrophysiol. **10**, 1087 (1999).
[4] J.J. Fox, R.F. Gilmour, Jr., and E. Bodenschatz, Phys. Rev. Lett. **89**, 198101 (2002).
[5] F.H. Fenton, E.M. Cherry, H.M. Hastings, and S.J. Evans, Chaos **12**, 852 (2002).
[6] J.B. Nolasco, and R.W. Dahlen, J. Appl. Phys. **25**, 191 (1968).
[7] M. Guevara, G. Ward, A. Shrier, and L. Glass, *Computers in Cardiology* (IEEE Computer Society, Silver Spring, MD, 1984), p. 167.
[8] M.R. Boyett and B.R. Jewell, J. Physiol. (London) **285**, 359 (1978).
[9] M.R. Franz, C.D. Swerdlow, L.B. Liem, and J. Schaefer, J. Clin. Invest. **82**, 972 (1988).
[10] V. Elharrar and B. Surawicz, Am. J. Phys. **244**, H782 (1983).
[11] G.M. Hall, S. Bahar, and D.J. Gauthier, Phys. Rev. Lett. **82**, 2995 (1999).
[12] I. Banville and R.A. Gray, J. Cardiovasc. Electrophysiol. **13**, 1141 (2002).
[13] E. Cytrynbaum and J.P. Keener, Chaos **12**, 788 (2002).
[14] J.J. Fox, E. Bodenschatz, and R.F. Gilmour Jr., Phys. Rev. Lett. **89**, 138101 (2002).
[15] E.M. Cherry and F.H. Fenton, Am. J. Phys. (to be published).
[16] R.F. Gilmour, N.F. Otani, and M.A. Watanabe, Am. J. Phys. **272**, H1826 (1997).
[17] N.F. Otani and R.F. Gilmour, Jr., J. Theor. Biol. **187**, 409 (1997).
[18] E.G. Tolkacheva, D.G. Schaeffer, D.J. Gauthier, and C.C. Mitchell, Chaos **12**, 1034 (2002).
[19] F. Fenton and A. Karma, Chaos **8**, 20 (1998).
[20] E.G. Tolkacheva, D.G. Schaeffer, D.J. Gauthier, and W. Krassowska, Phys. Rev. E **67**, 031904 (2003).
[21] K. Hall, D.J. Christini, M. Tremblay, J.J. Collins, L. Glass, and J. Billette, Phys. Rev. Lett. **78**, 4518 (1997).
[22] W.-J. Rappel, F. Fenton, and A. Karma, Phys. Rev. Lett. **83**, 456 (1999).
[23] D.J. Gauthier and J.E.S. Socolar, Phys. Rev. Lett. **79**, 4938 (1997).
[24] G.M. Hall and D.J. Gauthier, Phys. Rev. Lett. **88**, 198102 (2002).
[25] D.J. Christini, K.M. Stein, S.M. Markowitz, S. Mittal, D.J. Slotwiner, M.A. Scheiner, S. Iwai, and B.B. Lerman, Proc. Natl. Acad. Sci. U.S.A. **98**, 5827 (2001).
[26] E. Tolkacheva, M.M. Romeo, and D.J. Gauthier (unpublished).
[27] M.A. Watanabe, and M.L. Koller, Am. J. Phys. **282**, H1534 (2002).
[28] D.R. Chialvo, D.C. Michaels, and J. Jalife, Circ. Res. **66**, 525 (1990).
[29] F.H. Fenton, S.J. Evans, and H.M. Hastings, Phys. Rev. Lett. **83**, 3964 (1999).
[30] S.S. Kalb, H. Dobrovolny, E.G. Tolkacheva, S.F. Idriss, W. Krassowska, and D.J. Gauthier, J. Cardiovasc. Electrophysiol. (to be published).
[31] B. Echebarria and A. Karma, Phys. Rev. Lett. **88**, 208101 (2002).
[32] J.J. Fox, J.L. McHarg, and R.F. Gilmour Jr., Am. J. Phys. **282**, H516 (2002).
[33] J. Hale and H. Kocak, *Dynamics and Bifurcations* (Springer-Verlag, Berlin, 1991).
[34] For the mapping model (7) there are two ways of measuring the slope of the constant-BCL RC—measuring transients after a jump from one BCL value to another, and measuring transients after perturbations in BCL. The difference between these two kinds of constant-BCL RCs is one of the main subjects of our following paper. Note that both of these RCs are identical for the simpler mapping model (4). For the two-dimensional mapping model (7), we denote S_{bcl} as a slope of the RC containing transient values after perturbations in BCL.
[35] M.L. Koller, M.L. Riccio, and R.F. Gilmour, Jr., Am. J. Phys. **275**, H1635 (1998).